JOURNAL OF GEOPHYSICAL RESEARCH, VOL. 112, D03309, doi:10.1029/2006JD007258, 2007

Comparisons of Tropospheric Emission Spectrometer (TES) ozone profiles to ozonesondes: Methods and initial results

H. M. Worden,[1] J. A. Logan,[2] J. R. Worden,[1] R. Beer,[1] K. Bowman,[1] S. A. Clough,[3] A. Eldering,[1] B. M. Fisher,[1] M. R. Gunson,[1] R. L. Herman,[1] S. S. Kulawik,[1] M. C. Lampel,[4] M. Luo,[1] I. A. Megretskaia,[2] G. B. Osterman,[1] and M. W. Shephard[3]

Received 6 March 2006; revised 31 May 2006; accepted 30 August 2006; published 15 February 2007.

[1] The Tropospheric Emission Spectrometer (TES) on the Earth Observing System (EOS)-Aura spacecraft measures global profiles of atmospheric ozone with vertical resolution of 6–7 km in the troposphere for the nadir view. For a first validation of TES ozone measurements we have compared TES-retrieved ozone profiles to ozonesondes from fall, 2004. In some cases the ozonesonde data are from dedicated launches timed to match the Aura overpass, while other comparisons are performed with routine data available from the Southern Hemisphere Additional Ozonesonde (SHADOZ) archive and World Ozone and Ultraviolet Data Center (WOUDC) data archives. We account for TES measurement sensitivity and vertical resolution by applying the TES-averaging kernel and constraint to the ozonesonde data before differencing the profiles. Overall, for V001 data, TES ozone profiles are systematically higher than sondes in the upper troposphere but compare well in the lower troposphere, with respect to estimated errors. These comparisons show that TES is able to detect relative variations in the coarse vertical structure of tropospheric ozone.

Citation: Worden, H. M., et al. (2007), Comparisons of Tropospheric Emission Spectrometer (TES) ozone profiles to ozonesondes: Methods and initial results, *J. Geophys. Res.*, *112*, D03309, doi:10.1029/2006JD007258.

1. Introduction

[2] Distributions of the tropospheric column of ozone, as viewed from space, were first derived from measurements of total column ozone from the Total Ozone Measurement Spectrometer (TOMS) [*Fishman and Larsen*, 1987; *Fishman et al.*, 1990]. These observations provided valuable information about the global distribution of tropospheric ozone and the influence of biomass burning in the tropics. Estimates of tropospheric ozone from TOMS rely on various residual methods, in which the column of stratospheric ozone is subtracted from the total column of ozone, [e.g., *Fishman and Larsen*, 1987; *Hudson and Thompson*, 1998; *Ziemke et al.*, 1998, 2005]. The global distribution of tropospheric ozone has also been retrieved directly from the Global Ozone and Monitoring Experiment GOME [*Liu et al.*, 2005, 2006]. Neither of these observing methods provide vertical profiles of ozone. In order to investigate the mechanisms that control tropospheric ozone, vertical information is required.

[3] The Tropospheric Emission Spectrometer (TES) on EOS-Aura was designed to measure the global, vertical distribution of tropospheric ozone and ozone precursors such as carbon monoxide [*Beer et al.*, 2001; *Beer*, 2006]. In cloud-free conditions, the vertical resolution of TES nadir ozone estimates is about 6 km with sensitivity to both the lower and upper troposphere, as well as the stratosphere [*Bowman et al.*, 2002; *Worden et al.*, 2004].

[4] Ozonesondes fill a critical need for the validation of TES ozone profiles by providing in situ data from the surface to the stratosphere, with fine vertical resolution (~150 m). The primary challenge with using ozonesondes for TES validation is the relatively small number of acceptable coincident measurements for use in a statistical analysis. We apply an initial set of relatively loose coincidence criteria, described in section 2.3, followed by more selective criteria, based on temperature differences as discussed in section 4.2. These combined criteria result in a set of comparisons that are examined for statistical biases between TES and ozonesondes.

[5] To make comparisons between TES and ozonesondes, we must account for the vertical resolution and sensitivity of TES by applying the TES-averaging kernel and constraint to the sonde data. This results in a vertical profile that represents what TES would estimate for the atmospheric state as measured by the sonde and will be referred to as the sonde profile with the TES operator. Differences between TES ozone profiles and ozonesonde profiles with the TES operator are compared below to known systematic and random errors.

[1]Jet Propulsion Laboratory, California Institute of Technology, Pasadena, California, USA.
[2]Division of Engineering and Applied Sciences, Harvard University, Cambridge, Massachusetts, USA.
[3]Atmospheric and Environmental Research (AER), Lexington, Massachusetts, USA.
[4]Raytheon Information Solutions, Pasadena, California, USA.

0148-0227/07/2006JD007258$09.00

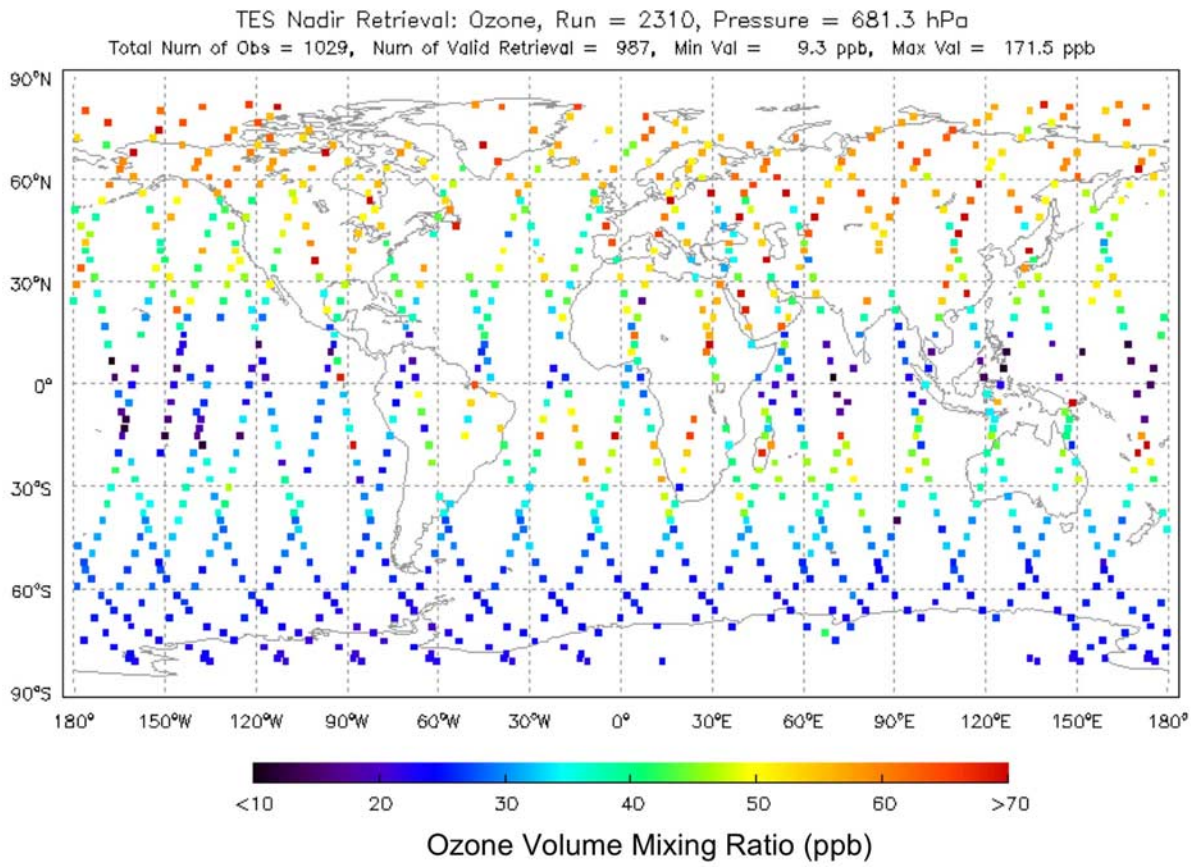

Figure 1. Example of a Tropospheric Emission Spectrometer (TES) Global Survey, showing estimated ozone values at 681.3 hPa. This map illustrates the coverage obtained in 16 orbits (~26 hours), in this case, starting on 10 November 2004. Boxes indicate measurement locations, but are larger than the actual TES footprint.

[6] The analysis presented in this paper is limited to observations between 20 September 2004 and 17 November 2004. The TES data used here, the V001 Beta Release, are available from the Langley Atmospheric Science Data Center (ASDC): http://eosweb.larc.nasa.gov/PRODOCS/tes/table_tes.html. Our purpose is to document the accuracy of the first release of TES data. The TES calibration has been improved over that used in the V001 Beta Release [*Worden et al.*, 2006]. Future validation efforts will use TES data with the updated calibration (V002), and cover a more extensive period of ozonesonde data. In order for the user to be able to explicitly account for vertical sensitivity when using or interpreting TES data, all the data versions include the averaging kernel and a priori constraint vector for each estimated profile.

2. Data

2.1. TES Data

[7] TES is a nadir and limb viewing infrared Fourier transform spectrometer (FTS) with an apodized resolution of around 0.10 cm^{-1} and a spectral range from 650 to 3250 cm^{-1}. The footprint of each nadir observation is 5 km by 8 km. TES is on the EOS-Aura platform [*Schoeberl et al.*, 2006] (http://aura.gsfc.nasa.gov/) in a near-polar, sun-synchronous, 705 km altitude orbit. The ascending node equator crossings are near 1:45 pm local solar time. The TES instrument and data acquisition modes are described by *Beer et al.* [2001] and *Beer* [2006]. The data used for these comparisons are nadir profiles only and include the first full 16-orbit Global Survey run, taken on 20 September 2004 and all subsequent Global Survey and Step/Stare runs up to 17 November 2004. Nadir observations for the Global Survey runs used here are about 5° apart along the orbit track, with successive orbits 22° apart in longitude. Step/Stare runs have denser nadir coverage, about 0.4° apart, and typically cover a 60° latitude range. Several of the TES Step/Stare runs were taken during the AVE (Aura Validation Experiment) campaign in Houston October–November 2004 where both aircraft (WB-57) and sonde data were collected. In all, eight Global Surveys and nine Step/Stares were used for this study. Representative data coverage over 16 orbits of Global Survey measurements is shown in Figure 1.

[8] Atmospheric ozone concentrations are estimated from the 9.6 μm ozone absorption band using a spectral range from 995 to 1070 cm^{-1}. The algorithms and spectral windows used for TES retrievals of atmospheric state

Table 1. Sonde Sites With Fall 2004 Tropospheric Emission Spectrometer (TES) Coincident Measurements Used for Analysis

Sonde Station	Latitude, °N	Longitude, °E	Number of Sondes Used	Number Timed for Aura Overpass	Distance Range, km	Time Difference, hours
Churchill	59	−94	1	0	159	43
Legionowo	52	21	1	0	238	12
Lindenberg	52	14	2	0	226, 375	13, 24
Hohenpeissenberg	48	11	3	0	232 − 483	18–20
Payerne	47	7	4	0	193 − 574	2–33
Trinidad Head	41	−124	2	0	208, 365	21, 34
Boulder	40	−105	2	0	93, 518	4, 44
Wallops	38	−76	2	0	247, 316	7, 18
Tateno	36	140	1	0	350	14
Huntsville (AVE)	35	−87	1	1	216	0.3
Kagoshima	32	131	2	0	276, 291	15, 27
Houston (AVE)	30	−95	4	4	145 − 720	0.1–1.2
Naha	26	128	2	0	154, 344	1,12
Hilo	20	−155	2	0	179, 480	36, 12
Sepang	3	102	1	0	285	3
Nairobi	−1	36	1	0	167	9
San Cristobal	−1	−90	2	0	295, 304	17, 31
Natal	−6	−35	4	3	158 − 520	1–4
Ascension	−8	−15	5	3	101 − 438	0.2–12
Samoa	−14	−170	1	0	265	19

parameters with corresponding error estimation are described by *Worden et al.* [2004] and *Bowman et al.* [2002, 2006]. TES retrievals use an optimal estimation approach following *Rodgers* [2000]. *Kulawik et al.* [2006b] show how individual TES profiles are characterized for errors and vertical information. Temperature and water vapor are retrieved concurrently with ozone. For operational simplicity, we set the initial guess to be equal to the a priori constraint in the retrieval. TES ozone retrievals use a priori profiles and covariance matrices from a climatology developed using the MOZART model [*Brasseur et al.*, 1998; *Park et al.*, 2004]. A priori information for temperature and water vapor is obtained from Goddard Space Flight Center (GSFC) Global Modeling and Assimilation Office (GMAO) [*Bloom et al.*, 2005].

[9] The TES data used in this analysis include both clear and cloudy nadir target scenes. The TES algorithms for modeling the atmospheric radiance and retrieving atmospheric parameters in the presences of clouds are described by *Kulawik et al.* [2006a]. TES nadir ozone profiles typically have a vertical resolution of around 6–7 km in the troposphere. The vertical resolution of tropospheric temperature is about 2–3 km. The primary diagnostic information used for screening failed retrievals in this analysis is the square of the radiance residual (data: forward model radiance), normalized by the NESR (Noise Equivalent Spectral Radiance), and is denoted as χ^2. Retrievals with $\chi^2 < 1.6$ were eliminated from the analysis.

2.2. Sonde Data

[10] Almost all the data used here were obtained using electrochemical concentration cell (ECC) ozonesondes, which rely on the oxidation reaction of ozone with potassium iodide in solution [*Komhyr et al.*, 1995]; the exceptions are sondes used at Hohenpeissenberg, Germany (Brewer Mast sondes) and those used in Japan (Kagoshima and Naha, type KC) (World Meteorological Organization (WMO), Assessment of Trends in the Vertical Distribution of Ozone, SPARC Report 1, WMO-Ozone Research and Monitoring Project Report 43, 1998, available at http://www.atmosp.physics.utoronto.ca/SPARC/; hereinafter referred to as WMO, 1998). The ozonesondes are flown with radiosondes, so that temperature data are also available. The sondes provide profiles to a maximum altitude of about 35 km (not all balloons reach this altitude) with vertical resolution of ∼150 m for ozone. The sonde data are provided in units of ozone partial pressure on a vertical scale of atmospheric pressure. The accuracy of the ozone measurement is about ±5% in the troposphere (WMO, 1998). Ozonesonde data used in this analysis were obtained from the World Ozone and Ultraviolet Data Center (WOUDC) (http://www.woudc.org), and the Southern Hemisphere Additional Ozonesonde (SHADOZ) archive (http://croc.gsfc.nasa.gov/shadoz). Most sonde stations make measurements weekly, but several in Europe make measurements 2–3 times a week. A few of the sondes used for validation were launched at the time of TES overpasses, including those from the AVE campaign [*Morris et al.*, 2006], and sondes from selected SHADOZ sites. Table 1 lists the sonde sites for the data used in these comparisons. Although more sondes were launched to coincide with Aura overpasses, and many other sites were checked for coincidences, only those passing both the initial criteria and the more restrictive temperature comparison criterion (discussed in section 4.2) are listed in Table 1.

[11] Most of the sonde data at the WOUDC have been normalized to the overhead column of ozone measured by a Dobson or Brewer instrument. The normalizing, or correction, factor (CF) was used here to screen the data. We included profiles for which the CF was in the range 0.85 to 1.15. The data provided at the SHADOZ archive have not been normalized [*Thompson et al.*, 2003]. We screened the SHADOZ data by integrating each sonde profile and comparing it to the ozone column from TOMS (Total Ozone Mapping Spectrometer) overpass data (http://toms.gsfc.nasa.gov); the amount of ozone above balloon burst is taken from a climatology which is an update of *McPeters et al.* [1997]. We eliminated from further analysis profiles for which the ratio of the integrated sonde/TOMS column differed from the mean value for that location by more than

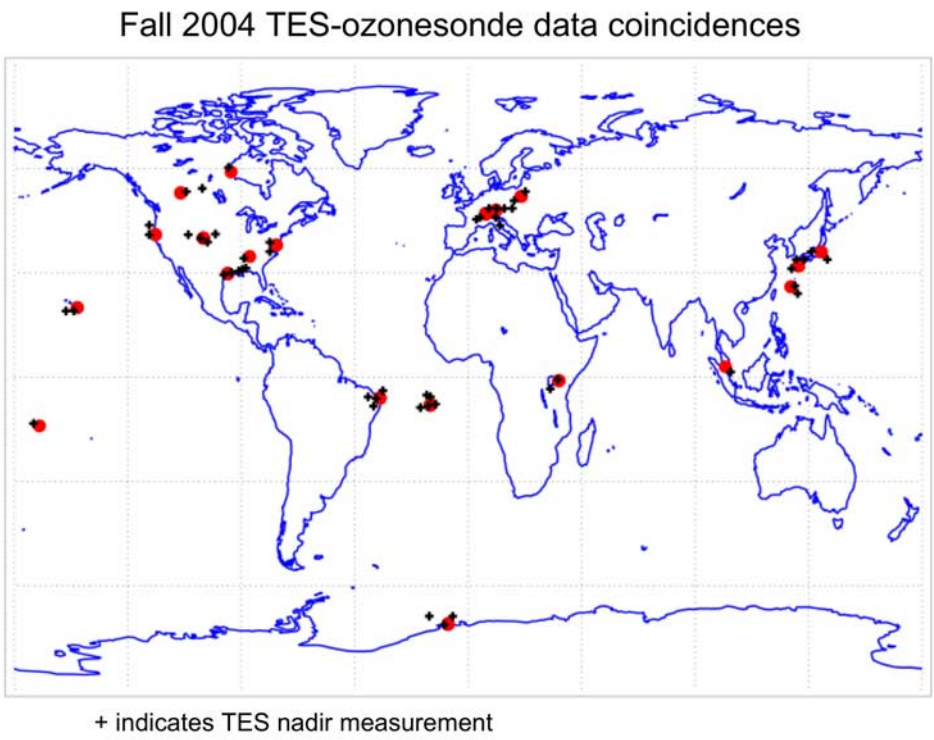

Figure 2. Map of TES − ozonesonde coincidences for 20 September 2004 to 17 November 2004. Red circles indicate sonde sites and + symbols indicate TES measurements. These matches satisfy the initial coincidence criteria, but not all pass the more selective criteria to be considered in statistical analysis.

15%. Although all the SHADOZ stations use ECC sondes, there are differences due to procedures, the solution strength of KI, and the instrument type (there are two manufacturers), as described by *Thompson et al.* [2003, 2007]. Consequently, when the integrated profiles are compared to TOMS column data there are station-to-station differences of up to 10%. These differences are small compared with the TES-sonde differences found below, but must be considered in future work as the TES calibration and retrieval is refined.

2.3. Coincidence Criteria

[12] Sonde–TES measurement pairs are selected using criteria required to obtain a sufficient number of matches for reasonable statistics. These criteria should be considered carefully with respect to expected scale dependencies for atmospheric variability. For example, *Sparling and Bacmeister* [2001] suggest a distance criterion of 100 km. However, applying this criterion we would obtain only three sonde-TES matches in this data set. Following the experience of previous satellite/sonde intercomparisons such as those with the Michelson Interferometer for Passive Atmospheric Sounding (MIPAS) on ENVISAT [*Steck et al.*, 2003; *Migliorini et al.*, 2004], we selected standard criteria of 600 km (TES measurement to sonde launch site) and 48 hours. To take advantage of all the sonde launches during the AVE campaign timed for the Aura overpass, we used a looser distance criterion of 800 km. Although these coincidence criteria might be more appropriate for stratospheric variability than for the troposphere, we found that tighter criteria yielded an insufficient number of matches for a meaningful analysis of the comparisons. Using these criteria for the September to November 2004 TES data gives 55 sonde-TES measurement pairs, shown in Figure 2. The refinement of these initial criteria is discussed in section 4.2.

3. Comparing In Situ and Remotely Sensed Data

3.1. Procedure for Sonde and TES Data Comparisons

[13] In order to compare TES profiles with in situ measurements, we must first account for the vertical smoothing and variable sensitivity inherent to trace gas and temperature profiles obtained by remote sensing, as shown in equation (1). Along with the sensitivity to the estimated parameters, the relative effect of the retrieval constraint vector, or a priori, varies with pressure. For each TES-sonde measurement pair, we apply the TES averaging kernel and constraint vector, or TES operator, to the sonde data, producing a profile that represents what TES would measure for the same air sampled by the sonde, in the absence of other error.

[14] The method of measurement intercomparison for remote sensing, accounting for averaging kernels and the a priori information used in the estimates, is described by *Rodgers* [2000] and *Rodgers and Connor* [2003], and was a critical step in the validation of MOPITT (Measurement of Pollution in the Troposphere) CO profiles [*Emmons et al.*, 2004]. We can neglect the averaging kernels associated with the sonde profiles since they are close enough to identity matrices due to vertical resolution (∼150 m) that is much finer than that of TES. As described in the equations below, the adjusted sonde profile, hereafter referred to as the sonde profile with TES operator (sonde w/TESop), can then be differenced with the corresponding TES profile and compared to estimated errors.

[15] Given a state vector **x,** in this case either temperature in K or ozone in logarithm of volume mixing ratio (VMR) as a function of pressure, the TES estimate can be written as the linear expression:

$$\hat{\mathbf{x}} = \mathbf{x}_{a\ priori} + \mathbf{A}_{\mathrm{xx}}\left[\mathbf{x} - \mathbf{x}_{a\ priori}\right] + \mathbf{Gn} + \delta_{cs} \tag{1}$$

where $\mathbf{x}_{a\ priori}$ is the a priori constraint vector, $\mathbf{n}$ is the spectral noise, $\mathbf{G}$ is the gain matrix, which describes the sensitivity of the estimate to the measured radiance with

$$\mathbf{G} = \frac{\partial \mathbf{x}}{\partial \mathbf{F}} = \left(\mathbf{K}^{\mathrm{T}}\mathbf{S}_{\mathrm{n}}^{-1}\mathbf{K} + \Lambda\right)^{-1}\mathbf{K}^{\mathrm{T}}\mathbf{S}_{\mathrm{n}}^{-1} \tag{2}$$

$\mathbf{F}$ is the forward model radiance, $\mathbf{K}$ is the Jacobian matrix, $\mathbf{S_n}$ is the measurement covariance, and Λ is the constraint matrix. These give the averaging kernel $\mathbf{A}_{\mathrm{xx}} = \mathbf{GK}$, which is the sensitivity of the retrieval to the true state. We also define the ''cross-state'' errors incurred from retrieving multiple parameters (e.g., temperature, water vapor and surface emissivity) as:

$$\delta_{cs} = \mathbf{A}_{cs}\left[\mathbf{x}_{cs} - \mathbf{x}_{cs_{a\ priori}}\right] \tag{3}$$

where $\mathbf{A}_{cs}$ is the submatrix of the averaging kernel for the full state vector of all jointly retrieved parameters that relates the sensitivity of $\mathbf{x}$ to $\mathbf{x}_{\mathrm{cs}}$, the vector of cross-state parameters and corresponding cross-state a priori constraint vector. (see *Worden et al.* [2004] and *Bowman et al.* [2006] for more details on notation and definitions.)

[16] The in situ measurement for the same atmospheric state $\mathbf{x}$ is:

$$\mathbf{x}_{sonde} = \mathbf{x} + \delta_{sonde} \tag{4}$$

with error vector δ_{sonde} for the sonde profile. (We assume the sonde errors have an uncorrelated, *i.e.*, diagonal only covariance). For sonde profiles that did not reach 10 hPa, the unmeasured part of the stratosphere is approximated by appending the TES a priori. For ozone, the TES a priori is scaled to the last available sonde point and for temperature it is shifted. The sonde data are interpolated and extrapolated to a fine level pressure grid (180 levels per decade pressure; 800 levels from 1260 hPa to 0.046 hPa). This ensures a robust mapping procedure since the pressure grids of the original sonde data are irregular and variable. The sonde profiles were then mapped to the 87 level pressure level grid, covering 1212 hPa to 0.1 hPa, used for TES profiles and averaging kernels with a mapping matrix ($\mathbf{M}^*$) that is the pseudo-inverse of the matrix ($\mathbf{M}$) that interpolates from the 87 TES pressure levels to the fine level pressure grid with $\mathbf{M}^* = (\mathbf{M}^{\mathrm{T}}\mathbf{M})^{-1}\,\mathbf{M}^{\mathrm{T}}$. The equivalent TES estimate for the sonde measurement, sonde w/TESop, is then:

$$\hat{\mathbf{x}}_{sonde} = \mathbf{x}_{a\ priori} + \mathbf{A}_{xx}\left[\mathbf{M}^*\mathbf{x}_{sonde} - \mathbf{x}_{a\ priori}\right] \tag{5}$$

We can now difference the TES (equation (1)) and sonde w/TESop (equation (5)) estimates:

$$\Delta_{TES-sonde} = \hat{\mathbf{x}} - \hat{\mathbf{x}}_{sonde} = \mathbf{A}_{\mathrm{xx}}[\mathbf{x} - \mathbf{M}^*\mathbf{x}_{sonde}] + \mathbf{Gn} + \delta_{cs} \tag{6}$$

For the following analysis, we only consider the differences in the troposphere. It is important to note that the difference above does not include the constraint vector $\mathbf{x}_{a\ priori}$, which simplifies the errors in the comparison. Because the difference is not biased by the a priori, we can use the comparisons to identify other biases in TES ozone profiles, such as those due to radiometric calibration error. The expected error for this difference is:

$$\begin{aligned}
&E\left[(\hat{\mathbf{x}} - \hat{\mathbf{x}}_{sonde})(\hat{\mathbf{x}} - \hat{\mathbf{x}}_{sonde})^T\right] = \\
&E\left[(\mathbf{A}_{\mathrm{xx}}[\mathbf{x} - \mathbf{M}^*\mathbf{x}_{sonde}] + \mathbf{Gn} + \delta_{cs})(\mathbf{A}_{\mathrm{xx}}[\mathbf{x} - \mathbf{M}^*\mathbf{x}_{sonde}] + \mathbf{Gn} + \delta_{cs})^T\right] = \\
&E\left[(\mathbf{A}_{\mathrm{xx}}\mathbf{M}^*\delta_{sonde})(\mathbf{A}_{\mathrm{xx}}\mathbf{M}^*\delta_{sonde})^T\right] + E\left[(\mathbf{Gn})(\mathbf{Gn})^T\right] + E\left[\delta_{cs}\delta_{cs}^T\right] = \\
&\underbrace{\mathbf{A}_{\mathrm{xx}}\mathbf{M}^*\mathbf{S}_{sonde}\mathbf{M}^{*T}\mathbf{A}_{\mathrm{xx}}^T}_{\text{Sonde error}} + \underbrace{\mathbf{G}\mathbf{S}_n\mathbf{G}^T}_{\substack{\text{TES meas.}\\ \text{error}}} + \underbrace{\mathbf{A}_{\mathrm{cs}}\mathbf{S}_{cs}\mathbf{A}_{\mathrm{cs}}^T}_{\substack{\text{TES cross}-\\ \text{state error}}}
\end{aligned} \tag{7}$$

where $\mathbf{S}_{sonde}$ is the sonde error covariance, $\mathbf{S}_{\mathrm{n}}$ is the spectral radiance measurement error covariance and $\mathbf{S}_{\mathrm{cs}}$ is a block diagonal matrix containing the (uncorrelated) a priori covariances for the other jointly retrieved parameters, e.g., *TATM* (atmospheric temperature) and H_2O (water vapor):

$$\mathbf{S}_{cs} = \begin{pmatrix} \mathbf{S}_{TATM} & 0 \\ 0 & \mathbf{S}_{H_2O} \end{pmatrix}. \tag{8}$$

[17] The main contributions to the difference error are the TES measurement and cross-state terms which vary with altitude, and can be as high as 15–20% (each) for ozone. The sum of measurement and cross-state errors is labeled the observational error, which is provided in TES V002 data products. For this analysis, we neglect the errors associated with the sonde measurements (±5%) since they are significantly smaller than the TES error terms. We also neglect the approximation of the stratosphere that is applied in some sonde cases since the effects to the troposphere are minor. The error for the TES-sonde difference assumes that both measure the same atmospheric state. This, of course, is not the case, and differences in the sampled atmosphere are examined further in the following sections.

3.2. TES Nadir Ozone-Averaging Kernel Examples

[18] Averaging kernels are essential for understanding TES estimated profiles because they show where the retrieval is most sensitive vertically and how information is smoothed, thus giving a measure of the vertical resolution. They are computed and reported for each TES profile and provide the means for intercomparisons as well as for data assimilation [*Jones et al.*, 2003]. Figure 3 shows examples of TES nadir ozone-averaging kernels for clear and cloudy conditions. These plots illustrate how vertical smoothing in TES retrievals combines the information from different altitudes. In particular, the ozone abundance in the stratosphere has a significant influence on the TES retrieval of ozone in the upper troposphere (magenta and dark blue lines). By contrast, the TES retrievals in the lower troposphere are relatively free of stratospheric influence (green lines).

4. Results

4.1. Comparison Examples

[19] To demonstrate the TES-sonde comparison method, we examine two particular cases to see the effects of the

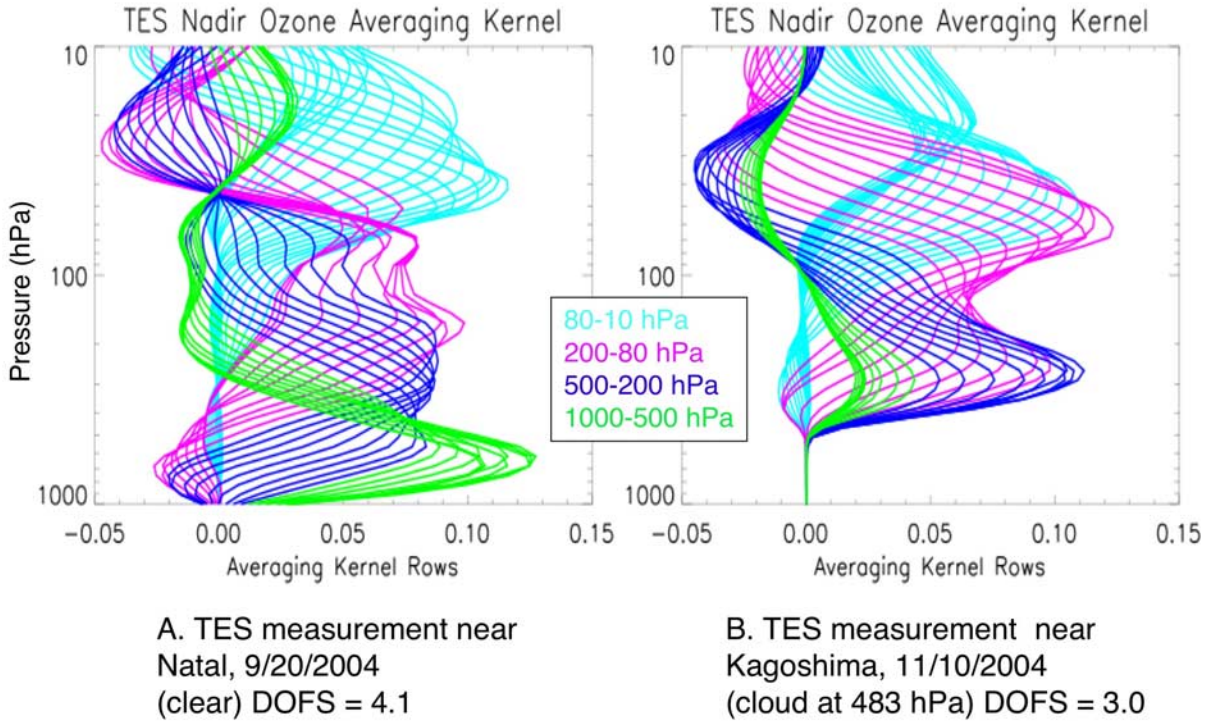

Figure 3. TES nadir ozone-averaging kernels under clear and cloudy conditions. The colors indicate averaging kernel rows corresponding to the pressure levels as noted in the legend.

TES operator (using equation (5)) on the input sonde data. Figure 4 shows the comparisons of TES data acquired on 11 October 2004 to a sonde launched from Ascension Island within an hour of the Aura overpass and TES data acquired on 10 November 2004 to a sonde launched a day earlier from Kagoshima. The corresponding TES ozone-averaging kernel is shown in Figure 3, right. Figure 4 shows how the fine vertical structure of the original sonde data is smoothed

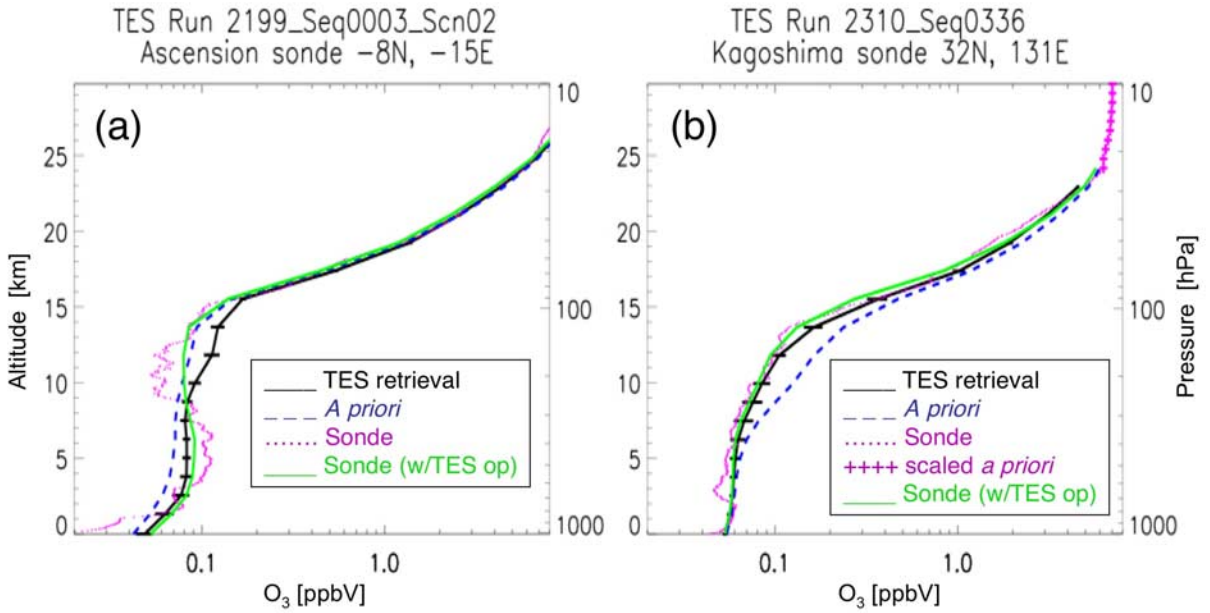

Figure 4. TES and ozonesonde comparisons for (a) TES measurement on 11 October 2004 separated by 229 km from Ascension Island sonde launched for the Aura overpass (less than 1 hour time difference) and (b) TES measurement on 10 November 2004 with sonde from Kagoshima launched a day earlier (separated by 291 km). The corresponding TES-averaging kernel is shown in Figure 3, right, with cloud observed at 483 hPa. Extension of the original sonde profile above 23.7 hPa, by scaling the ozone initial guess to match the last available sonde value, was performed in this case.

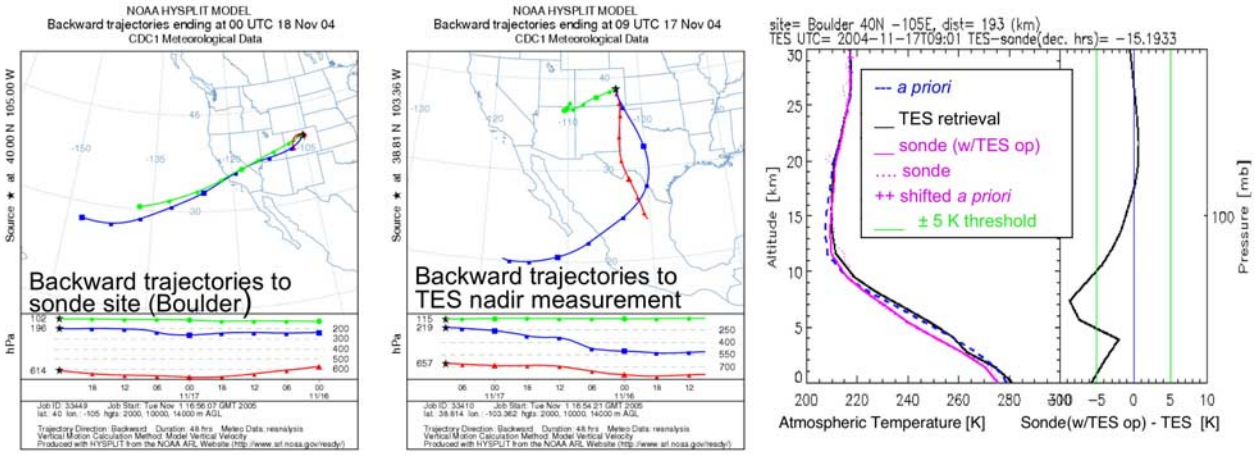

Figure 5. Backward trajectories at 2, 10 and 14 km above ground level (AGL) to sonde site (left) and TES measurement location (middle) with corresponding sonde (w/TESop) – TES temperature profile comparison (right) for a TES measurement 193 km from Boulder on 17 November 2004. Sonde data were acquired 15 hours later.

by the averaging kernel. In the altitude range below the observed cloud in the Kagoshima case, where TES has no sensitivity, both TES and sonde with TES operator profiles have the values of the a priori. Since the Kagoshima sonde data had a minimum pressure of 23.7 hPa, the top of the profile was extended by scaling the a priori to match the last available sonde value. Applying the same method, TES and sonde temperature profiles are also compared.

4.2. Trajectory Analysis and Temperature Difference Criterion

[20] In order to understand which comparisons are appropriate within the coincidence criteria used in our initial selection of TES measurement with sonde matches, we have performed backward trajectories for the locations and times of several TES and sonde measurement pairs. The trajectories are computed with the HYSPLIT transport and dispersion model (R. R. Draxler and G. D. Rolph, Hybrid Single-Particle Lagrangian Integrated Trajectory Model (HYSPLIT), 2006, available at NOAA Air Resources Laboratory Real-time Environmental Applications and Display System (READY) Web site (G. D. Rolph, 2003), http://www.arl.noaa.gov/ready/hysplit4.html). We found that there was a distinct relationship between cases with poor temperature comparisons (several pressure levels with >5 K differences between TES and sonde in the troposphere) and trajectories that represented obviously different source regions, as shown in Figure 5. In contrast, Figure 6 shows a case where the temperature difference falls within the criteria for an acceptable match (<5 K differences in the troposphere) and the corresponding similar back trajectories. We therefore use sonde-TES temperature differences as an additional

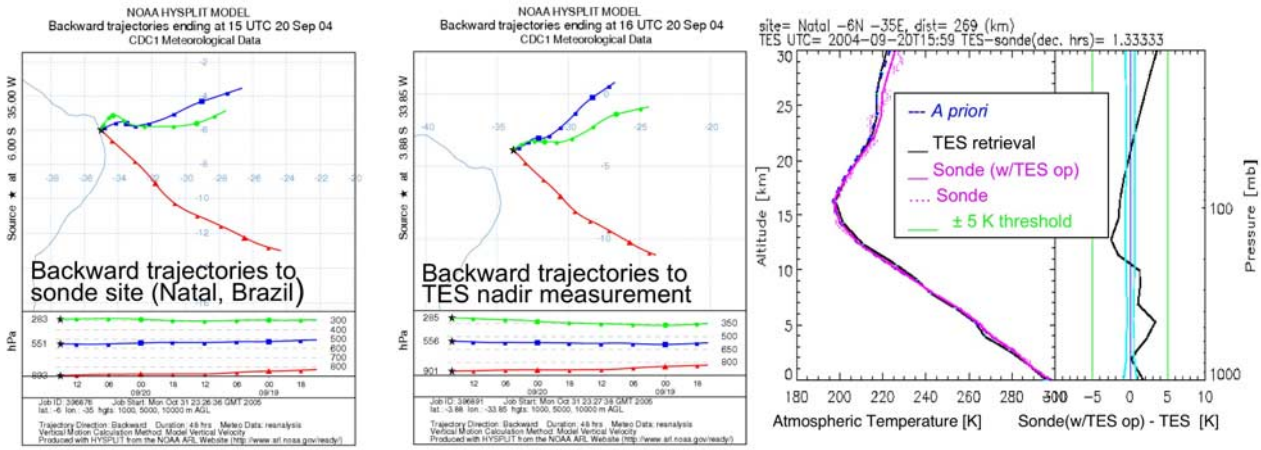

Figure 6. Backward trajectories at 1, 5, and 10 km above ground level (AGL) to sonde site (left) and TES measurement location (middle) with corresponding sonde (w/TESop) – TES temperature profile comparison (right) for a TES measurement 269 km from Natal on 20 September 2004. Sonde data were acquired 1.3 hours earlier.

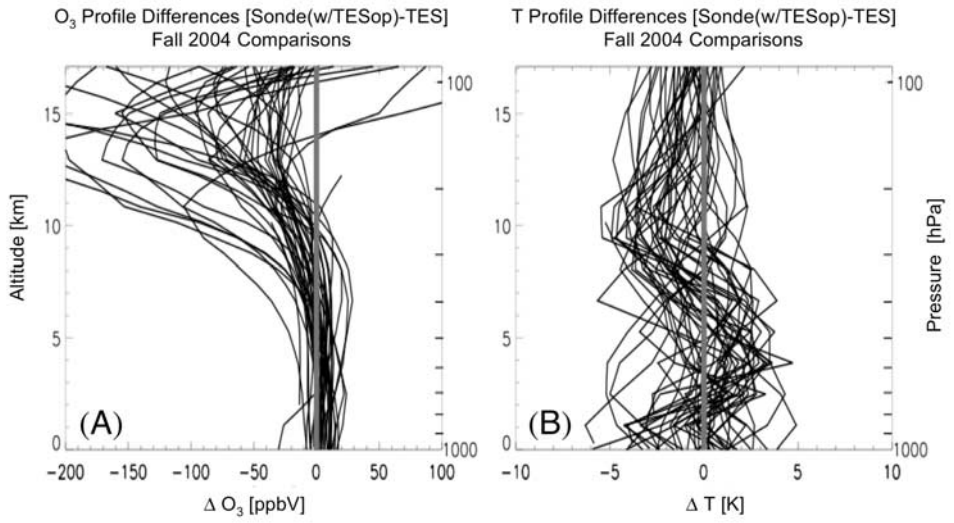

Figure 7. Sonde (w/TESop)−TES profile differences for 44 comparisons (cases passing the more selective criteria) with (a) ozone and (b) temperature.

filter to select comparison cases for the statistical analysis that follows.

4.3. Ensemble Results

[21] When we apply the temperature difference criteria described above, and exclude latitudes >60° where TES measurements are less reliable because of poor surface characterization, we are left with 43 coincident pairs, listed in Table 1. These represent a range of latitudes and cloud cover conditions. There were three cases, all in the northern midlatitudes, with high thick clouds obscuring the lower troposphere (effective cloud optical depth >3 at pressures less than 750 hPa). These cases were excluded from the statistics for the lower troposphere. Three other cases had low thick clouds (cloud top pressure >750 hPa). All other cases had effective cloud optical depths ranging from 0.01 to 1.3, with corresponding effects to TES sensitivity in the lower troposphere. Under these varying cloud conditions, the application of the TES operator to the sonde data ensures that the comparisons are unbiased by the TES a priori.

[22] Figure 7 shows an ensemble plot of all 43 sonde (w/TESop)-TES ozone profile differences in ppb and the corresponding temperature profile differences in Kelvin (K). The figure reveals a clear bias, with TES measuring higher ozone in the upper troposphere, peaking around 200 hPa. There are also systematic temperature biases − the TES temperatures too high in the upper troposphere and too low in the lower troposphere. The temperature bias is corroborated by other comparisons to radiosondes and AIRS retrievals (G. B. Osterman (Ed.), TES Validation Report, version 1.00 (available at http://eosweb.larc.nasa.gov/PRODOCS/tes/table_tes.html), and is discussed below in terms of the effects of a calibration error in section 5.

4.3.1. Tropics and Midlatitude Characteristics

[23] Figure 8 compares vertical averages of TES and sonde with the TES operator data so that we can summarize TES ozone estimates for different latitudes and ozone abundance conditions. The plots show unweighted averages over TES vertical levels in the lower troposphere (surface to 500 hPa) and upper troposphere (500 hPa to tropopause or 200 hPa, whichever is at higher pressure). The tropopause pressures are computed by fitting the TES temperature profile minima, and they range from 300 hPa (higher latitudes) to 100 hPa for the tropics. In order to minimize the influence of the stratosphere in the upper troposphere, due to the averaging kernel, we set the minimum pressure for the averages at 200 hPa. Results are also shown separately for the tropics (latitude <25°) and midlatitudes (25° > latitude > 60°). The figure includes the mean bias and root mean square (rms) of the differences. There is clearly a linear relationship between TES and sonde measurements in the tropics, for both the upper and lower troposphere, and in the upper troposphere at midlatitudes. This is the case even though the upper tropospheric bias in each region is larger than the TES measurement and cross-state errors. This linearity gives confidence to users of TES data that relative variations as observed on a global map are significant, even though biased.

4.3.2. Correlations of Error-Weighted Differences

[24] In order to test our assumptions for coincidence criteria, we calculate the error-weighted differences between the sonde with TES operator and TES profiles, averaged for the upper and lower troposphere, denoted as $|\langle \Delta_{TES\text{-}sonde} \rangle|_{\sigma}$. The difference $\Delta_{TES\text{-}sonde}$ is defined in equation (6), with averaging over pressures indicated by $\langle\ \rangle$. The vertical bars indicate magnitude values and subscript σ indicates that the difference is divided by the diagonal error from the terms in equation (7) for TES measurement and cross-state errors. The error weighting allows us to test for correlations in the ozone differences while accounting for the possible dependence on TES measurement errors. We have found only weak correlations, listed in Table 1, for ozone differences with distance and time coincidence criteria, although this could be due to the small number of comparisons. These low correlations suggest that our bias is dominant over differences that might be expected from horizontal-scale variations. We have also considered correlations with the TES retrieved cloud top pressure. Although these correlations are negative as

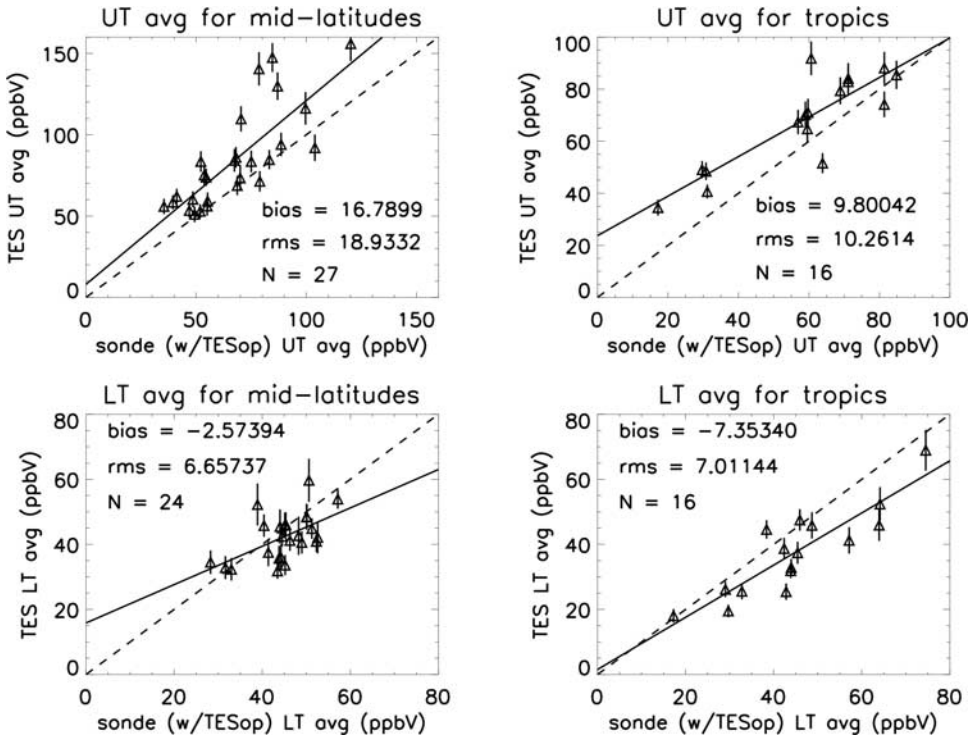

Figure 8. Comparisons of TES (with error bars) and sonde with TES operator average abundances. The four panels show upper troposphere (UT) averages (500 hPa to tropopause or 200 hPa, whichever is at higher pressure) separated for midlatitudes (25° < latitude < 60°) and tropics (latitude < 25°) and lower-troposphere (LT) averages (surface to 500 hPa) separated for midlatitudes and tropics. Dashed lines show the 1:1 reference. TES-sonde (w/TESop) bias and RMS values, in ppbV are shown for the N number of cases in each panel. Three cases were excluded for midlatitude LT due to optically thick clouds above 750 hPa.

expected; that is, higher clouds (lower pressure) would interfere more with the comparison, they are also relatively weak. For comparison, the correlations for the pressure averaged TES and sonde with TES operator abundances, shown in Figure 8, are given in the last row of Table 2.

4.4. Sensitivity to Profile Shape

[25] Finally, we use ozonesonde-TES comparisons to determine if TES measurements can differentiate large-scale profile features, such as enhancements due to biomass burning downwind of source regions such as those observed routinely at Ascension Island. [*Thompson et al.*, 1996]. Figure 9 shows the comparison of three ozonesonde profiles (two from Natal and one from Ascension), the corresponding comparison of the closest TES measurements and the a priori used for the TES retrievals, where differences in the latter are due only to changes in the monthly climatology data. It is clear that even with a bias in the upper troposphere, TES is sensitive to the enhanced tropospheric ozone observed at Ascension. Figure 10 shows a similar comparison for sonde and TES profiles at subtropical and midlatitudes and demonstrates TES sensitivity to the different ozone gradients corresponding to latitudinal variations in tropopause height.

5. Expected Calibration Improvements

[26] The TES radiance spectra used for these comparisons (V001) have known calibration errors that will be corrected in the next data version, [*Worden et al.*, 2006]. For one TES Global Survey, run 2147, taken 20 September 2005, we have processed the data with an improved L1B calibration algorithm and we examine the expected changes for ozonesonde comparisons with V002 data. The primary validation for TES radiances is a comparison with measurements from AIRS on EOS-Aqua [*Pagano et al.*, 2003], taken about 12 minutes earlier along the same orbit. TES spectral data are convolved with the AIRS spectral response function (SRF) before the comparison is made. For the data set used in this study, there are differences >1 K in brightness temperature for the TES-AIRS comparisons. Improved calibration algorithms reduce this to better than 0.5 K. An example of the resulting changes to the ozone retrievals is shown in Figure 11. Only three cases were available for comparing with ozonesonde data, but all showed significant

Table 2. Correlations of TES: Sonde with TES Operator Differences With Distance, Time Difference, and Retrieved Cloud Top Pressure

Correlation Pair ⟨a,b⟩	Upper Troposphere correlation	Lower Troposphere Correlation
$\langle\lvert\langle\Delta_{TES\text{-}sonde}\rangle\rvert_{\sigma}$, |distance|⟩	−0.15	0.03
$\langle\lvert\langle\Delta_{TES\text{-}sonde}\rangle\rvert_{\sigma}$, |time_difference|⟩	0.08	−0.25
$\langle\lvert\langle\Delta_{TES\text{-}sonde}\rangle\rvert_{\sigma}$, cloud top pressure⟩	−0.09	−0.02
⟨⟨TES⟩,⟨sonde w/TESop⟩⟩	0.80	0.76

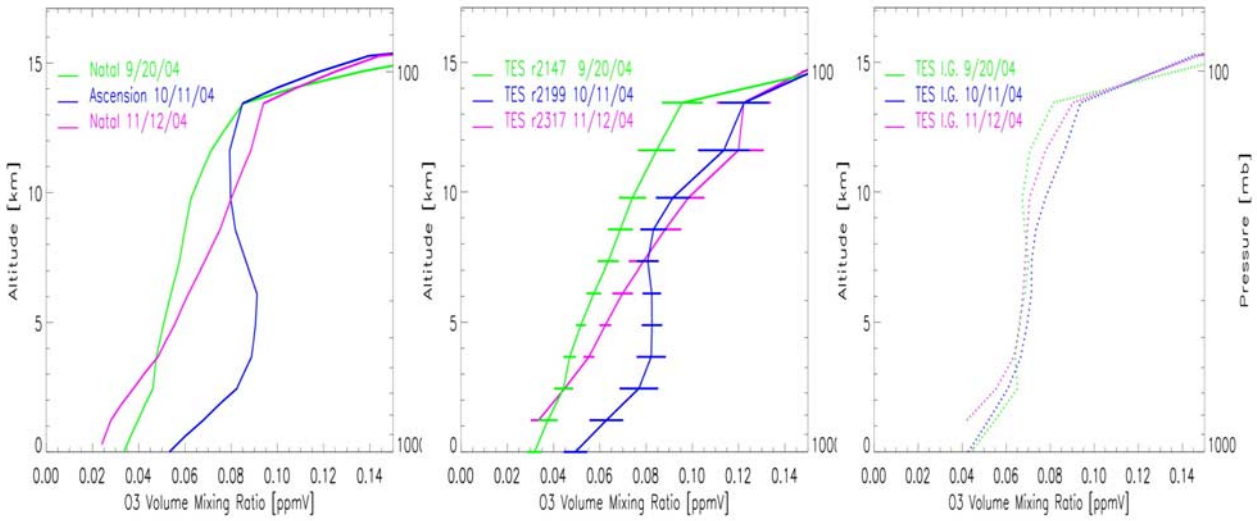

Figure 9. Tropical ozone profiles from ozonesondes with TES operator (left), TES retrievals (middle) and for reference, TES a priori (right) from the MOZART climatology (same as initial guess, I.G.).

decreases in both temperature and ozone biases, especially in the upper troposphere. This was expected since the calibration corrections were largest for lower radiance values, such as those emitted near the tropopause.

6. Conclusions and Outlook

[27] We have established that TES V001 ozone retrievals in the upper troposphere are biased high compared to sonde measurements. Despite this bias, TES is able to distinguish between high and low ozone abundances in both the lower and upper troposphere and can detect large-scale features in ozone profiles.

[28] We plan further validation of the TES ozone product using TES retrievals with the improved calibration discussed in section 5. Future TES-sonde comparisons will have better statistics because of increased nadir sampling for the TES Global Survey mode since 21 May 2005. Nadir scans are now spaced $\sim$1.6° along the orbit track, instead of every 5°, which is the spatial sampling of the earlier TES nadir data, such as shown in Figure 1. This increase was at the expense of routine limb observations, but has significantly improved the number of useful tropospheric ozone measurements. In our future work, we expect to be able to use stricter spatial and temporal criteria for matches, in part because of the higher frequency of TES nadir sampling, which should lead to more matches with routine ozonesonde launches and also because sondes are being launched coincident with Aura overpasses as part of planned validation campaigns. We

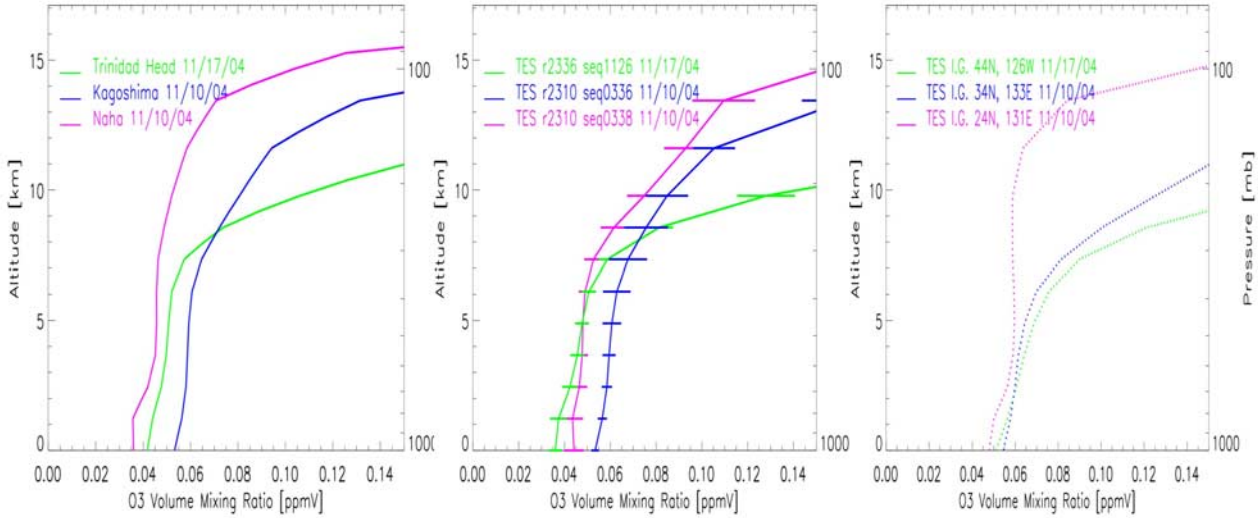

Figure 10. Subtropical and midlatitude ozone profiles from ozonesondes with TES operator (left), TES retrievals (middle) and for reference, TES a priori (right) from the MOZART climatology (same as initial guess, I.G.).

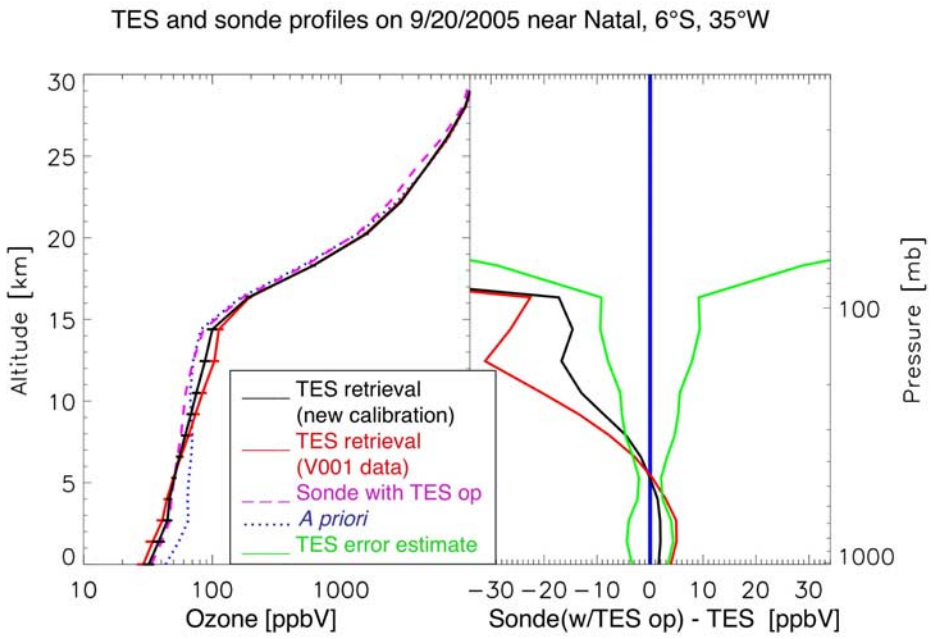

Figure 11. Example of changes to the ozone retrieval and comparison to sonde for the improved L1B calibration to be applied for TES V002 data.

will also examine the role of natural variability in influencing sonde-TES differences.

[29] **Acknowledgments.** This work was performed, in part, at the Jet Propulsion Laboratory, California Institute of Technology, under a contract with the National Aeronautics and Space Administration. J.A.L. and I.A.M. were funded by a grant from NASA to Harvard University. The authors gratefully acknowledge Frank Schmidlin, Michael Newchurch, and Gary Morris for dedicated sonde launches corresponding to Aura overpasses. Gary Morris of Valparaiso University had sponsorship for A.V.E. (Aura Validation Experiment) from the Shell Center for Sustainability and NASA's IONS program. We also thank the World Ozone Data Centre and the SHADOZ program for making the routine sonde data accessible and the NOAA Air Resources Laboratory (ARL) for the provision of the HYSPLIT transport and dispersion model used in this analysis (http://www.arl.noaa.gov/ready/hysplit4.html).

References

Beer, R. (2006), TES on the Aura Mission: Scientific Objectives, Measurements and Analysis Overview, *IEEE Trans. Geosci. Remote Sens.*, *44*(5), 1102.

Beer, R., T. A. Glavich, and D. M. Rider (2001), Tropospheric Emission Spectrometer for the Earth Observing System's Aura satellite, *Appl. Opt.*, *40*, 2356–2367.

Bloom, S., et al. (2005), *Documentation and Validation of the Goddard Earth Observing System (GEOS) Data Assimilation System—Version 4*, *Tech. Rep. Ser. on Global Model. and Data Assim. NASA/TM-2005-104606*, vol. 26, 187 pp. (Available at http://gmao.gsfc.nasa.gov/pubs/docs/Bloom168)

Bowman, K. W., T. Steck, H. M. Worden, J. Worden, S. Clough, and C. Rodgers (2002), Capturing time and vertical variability of tropospheric ozone: A study using TES nadir retrievals, *J. Geophys. Res.*, *107*(D23), 4723, doi:10.1029/2002JD002150.

Bowman, K. W., et al. (2006), Tropospheric Emission Spectrometer: Retrieval method and error analysis, *IEEE Trans. Geosci. Remote Sens.*, *44*(5), 1297.

Brasseur, G. P., D. A. Hauglustaine, S. Walters, P. J. Rasch, J. F. Muller, C. Granier, and X. X. Tie (1998), MOZART, a global chemical transport model for ozone and related chemical tracers 1: Model description, *J. Geophys. Res.*, *103*, 28,265–28,289.

Emmons, L. K., et al. (2004), Validation of Measurements of Pollution in the Troposphere (MOPITT) CO retrievals with aircraft in situ profiles, *J. Geophys. Res.*, *109*, D03309, doi:10.1029/2003JD004101.

Fishman, J., and J. C. Larsen (1987), Distribution of total ozone and stratospheric ozone in the tropics: Implications for the distribution of tropospheric ozone, *J. Geophys. Res.*, *92*, 6627–6634.

Fishman, J., C. E. Watson, J. C. Larsen, and J. A. Logan (1990), The distribution of tropospheric ozone obtained from satellite data, *J. Geophys. Res.*, *95*, 3599–3617.

Hudson, R. D., and A. M. Thompson (1998), Tropical tropospheric ozone from Total Ozone Mapping Spectrometer by a modified residual method, *J. Geophys. Res.*, *103*, 22,129–22,145.

Jones, D. B. A., K. W. Bowman, P. I. Palmer, J. R. Worden, D. J. Jacob, R. N. Hoffman, I. Bey, and R. M. Yantosca1 (2003), Potential of observations from the Tropospheric Emission Spectrometer to constrain continental sources of carbon monoxide, *J. Geophys. Res.*, *108*(D24), 4789, doi:10.1029/2003JD003702.

Komhyr, W. D., R. A. Barnes, G. B. Brothers, J. A. Lathrop, and D. P. Opperman (1995), Electrochemical concentration cell ozonesonde performance evaluation during STOIC 1989, *J. Geophys. Res.*, *100*, 9231–9244.

Kulawik, S. S., J. Worden, A. Eldering, K. Bowman, M. Gunson, G. B. Osterman, L. Zhang, S. A. Clough, M. W. Shephard, and R. Beer (2006a), Implementation of cloud retrievals for Tropospheric Emission Spectrometer (TES) atmospheric retrievals. part I: Description and characterization of errors on trace gas retrievals, *J. Geophys. Res.*, *111*, D24204, doi:10.1029/2005JD006733.

Kulawik, S. S., et al. (2006b), TES atmospheric profile retrieval characterization: An orbit of simulated observations, *IEEE Trans. Geosci. Remote Sens.*, *44*(5), 1324.

Liu, X., K. Chance, C. E. Sioris, R. J. D. Spurr, T. P. Kurosu, R. V. Martin, and M. J. Newchurch (2005), Ozone profile and tropospheric ozone retrievals from the Global Ozone Monitoring Experiment: Algorithm description and validation, *J. Geophys. Res.*, *110*, D20307, doi:10.1029/2005JD006240.

Liu, X., et al. (2006), First directly retrieved global distribution of tropospheric column ozone from GOME: Comparison to the GEOS-Chem model, *J. Geophys. Res.*, *111*, D02308, doi:10.1029/2005JD006564.

McPeters, R. D., G. J. Labow, and B. J. Johnson (1997), A satellite-derived ozone climatology for balloon sonde estimation of total column ozone, *J. Geophys. Res.*, *102*, 8875–8885.

Migliorini, S., C. Piccolo, and C. D. Rodgers (2004), Intercomparison of direct and indirect measurements: Michelson Interferometer for Passive Atmospheric Sounding (MIPAS) versus sonde ozone profiles, *J. Geophys. Res.*, *109*, D19316, doi:10.1029/2004JD004988.

Morris, G. A., et al. (2006), Alaskan and Canadian forest fires exacerbate ozone pollution over Houston, Texas, on 19 and 20 July 2004, *J. Geophys. Res.*, *111*, D24S03, doi:10.1029/2006JD007090.

Pagano, T. S., H. H. Aumann, D. Hagan, and K. Overoye (2003), Prelaunch and in-flight radiometric calibration of the Atmospheric Infrared Sounder (AIRS), *IEEE Trans. Geosci. Remote Sens.*, *41*, 265–273.

Park, M., W. J. Randel, D. E. Kinnison, R. R. Garcia, and W. Choi (2004), Seasonal variations of methane, water vapor, ozone, and nitrogen dioxide near the tropopause: Satellite observations and model simulations, *J. Geophys. Res.*, *109*, D03302, doi:10.1029/2003JD003706.

Rodgers, C. (2000), *Inverse Methods for Atmospheric Sounding: Theory and Practise*, World Sci., Hackensack, N. J.

Rodgers, C. D., and B. J. Connor (2003), Intercomparison of remote sounding instruments, *J. Geophys. Res.*, *108*(D3), 4116, doi:10.1029/2002JD002299.

Schoeberl, M. R., et al. (2006), Overview of the EOS Aura Mission, *IEEE Trans. Geosci. Remote Sens.*, *44*(5), 1066.

Sparling, L. C., and J. T. Bacmeister (2001), Scale dependence of tracer microstructure: PDFs, intermittency and the dissipation scale, *Geophys. Res. Lett.*, *28*, 2823–2826.

Steck, T., et al. (2003), Validation of ozone measurements from MIPAS-ENVISAT: First results, poster, 11th International Workshop on Atmospheric Science from Space Using Fourier Transform Spectrometry (ASSFTS), Inst. für Meteorol. und Klimaforsch. (IMK), Forsch. Karlsruhe, Bad Wildbad, Germany, 8–10 Oct.

Thompson, A. M., et al. (1996), Where did tropospheric ozone over southern Africa and the tropical Atlantic come from in October, 1992?: Insights from TOMS, GTE/TRACE-A and SAFARI-92, *J. Geophys. Res.*, *101*, 24,251–24,278.

Thompson, A. M., et al. (2003), The 1998–2000 SHADOZ (Southern Hemisphere Additional Ozonesondes) tropical ozone climatology: Comparisons with TOMS and ground-based measurements, *J. Geophys. Res.*, *108*(D2), 8238, doi:10.1029/2001JD000967.

Thompson, A. M., J. C. Witte, H. G. J. Smit, S. J. Oltmans, B. J. Johnson, V. W. J. H. Kirchhoff, and F. J. Schmidlin (2007), The Southern Hemisphere Additional Ozonesondes (SHADOZ) 1998–2004 tropical ozone climatology: 3. Instrumentation, station-to-station variability, and evaluation with simulated flight profiles, *J. Geophys. Res.*, doi:10.1029/2005JD007042, in press.

Worden, H., R. Beer, K. Bowman, B. Fisher, M. Luo, D. Rider, E. Sarkissian, D. Tremblay, and J. Zong (2006), TES level1 algorithms: Interferogram processing, geolocation, radiometric and spectral calibration, *IEEE Trans. Geosci. Remote Sens.*, *44*(5), 1288–1296.

Worden, J., S. S. Kulawik, M. Shepard, S. Clough, H. Worden, K. Bowman, and A. Goldman (2004), Predicted errors of Tropospheric Emission Spectrometer nadir retrievals from spectral window selection, *J. Geophys. Res.*, *109*, D09308, doi:10.1029/2004JD004522.

Ziemke, J. R., S. Chandra, and P. K. Bhartia (1998), Two new methods for deriving tropospheric column ozone from TOMS measurements: Assimilated UARS MLS/HALOE and convective-cloud differential techniques, *J. Geophys. Res.*, *103*, 22,115–22,127.

Ziemke, J. R., S. Chandra, and P. K. Bhartia (2005), A 25-year data record of atmospheric ozone in the Pacific from Total Ozone Mapping Spectrometer (TOMS) cloud slicing: Implications for ozone trends in the stratosphere and troposphere, *J. Geophys. Res.*, *110*, D15105, doi:10.1029/2004JD005687.

R. Beer, K. Bowman, A. Eldering, B. M. Fisher, M. R. Gunson, R. L. Herman, S. S. Kulawik, M. Luo, G. B. Osterman, H. M. Worden, and J. R. Worden, Jet Propulsion Laboratory, California Institute of Technology, 4800 Oak Grove Drive, Pasadena, CA 91109, USA. (helen.worden@jpl.nasa.gov)

S. A. Clough and M. W. Shephard, Atmospheric and Environmental Research, (AER), 131 Hartwell Avenue, Lexington, MA 02420, USA.

M. C. Lampel, Raytheon Information Solutions, 299 N. Euclid Avenue, Suite 500, Pasadena CA, 91101, USA.

J. A. Logan and I. A. Megretskaia, Division of Engineering and Applied Sciences, Harvard University, Pierce Hall, 29 Oxford Street, Harvard University, Cambridge, MA 02138, USA.